COBEM 2023 27TH INTERNATIONAL CONGRESS OF MECHANICAL ENGENEERING

ABCM Brazilian Society of Mechanical Sciences and Engineering
27th ABCM International Congress of Mechanical Engineering
December 04-08, 2023, Florianópolis-SC, Brazil

COB-2023-1761
MODELING AND SIMULATION OF A HYBRID PHOTOVOLTAIC/THERMAL SYSTEM WITH A FRESNEL LINEAR CONCENTRATOR (CPVT)
27th COBEM

Pedro Moreira da Silva Neto
Darío Gerardo Fantini
Mário Benjamin Baptista de Siqueira
University of Brasília, Faculdade de Tecnologia, Mechanical Engineering Department, Caixa Postal 4399, 70910-900, Brasília-DF, Brazil

moreira.neto@aluno.unb.br, dario.fantini@aluno.unb.br, mariosiqueira@unb.br

Abstract. *Due to the need to reduce the use of fossil fuels for electricity and/or heat production, the search for renewable energy sources has been growing recently, with the Sun being a promising candidate as a renewable energy source. In this context, hybrid photovoltaic-thermal systems are interesting for simultaneously supplying electricity and heat demand, and these systems can be with solar concentration - using reflective mirrors or converging lens. In this sense, this work aims to show aspects of optical and thermal modeling, through computational simulation, and a prototype photovoltaic-thermal system with linear Fresnel reflectors (CPVT-LFR) designed to operate in the Laboratory of Energy and Environment (LEA) at the University of Brasília. The system consists of solar concentration using Linear Fresnel reflectors, which focus solar radiation onto a set of water-cooled monocrystalline silicon photovoltaic cells. The simulation results show that the maximum value obtained for electrical efficiency was 10%, while the thermal efficiency reached 83%, the cell temperature remained below 100°C, and the fluid temperature at the outlet could exceed 40°C. Furthermore, initial tests with the prototype showed positive results for concentration in the absorber.*

Keywords: *Hybrid Photovoltaic Thermal System, Solar Concentration, CPVT, Linear Fresnel Reflectors, Water Cooling.*

1. INTRODUCTION

Carbon dioxide (CO2) is one of the main contributors to the greenhouse effect, and the increase in CO2 emissions is closely related to the rise in energy consumption. According to the International Energy Agency (IEA), half of the increase in energy consumption in 2018 was attributed to higher electricity consumption. In terms of thermal energy, it is known that 40% of global CO2 emissions occur due to water heating and space heating in buildings, as well as industrial processes. Therefore, several organizations promote policies to reduce CO2 emissions, including the IEA and the United Nations (UN).

The Sun is an excellent candidate to be the primary renewable energy source, as the solar energy that reaches the planet in one hour is greater than the total energy consumed by Earth in a year (Lewis, 2007). However, scientists and engineers face technological challenges in harnessing solar resources efficiently. Among the technologies for harnessing solar energy is the hybrid photovoltaic-thermal system with Linear Fresnel concentration (CPVT-LFR). This system has the advantage of producing two forms of energy: electric energy (through photovoltaic cells) and thermal energy (through the heat absorbed by a fluid in the cell cooling process). Thus, the CPVT-LFR system achieves higher overall efficiency when compared to traditional photovoltaic systems and is economically more viable, as it reduces the area of solar cells required to generate the same electric power. Additionally, the cost of photovoltaic cells is much higher than that of mirrors for solar concentration. However, the CPVT-LFR system has a more complex construction and its commercial utilization is lower compared to the photovoltaic system.

According to the Instituto Nacional de Pesquisas Espaciais (INPE) - which produced the Atlas Brasileiro de Energia Solar - the city of Brasília is part of the region known as the "Cinturão Solar." This region, which stretches from the Northeast of Brazil to the Pantanal, exhibits above-average levels of solar irradiation throughout the year. Additionally, the regions within the solar belt experience a dry season from May to September, reducing the issues of rainy days and cloudiness, which can decrease the efficiency of solar resource utilization. In this regard, the present study aims to evaluate the generation of electric and thermal energy in a CPVT-LFR system designed for the Laboratory of Energy and Environment (LEA) at the University of Brasília (UnB), showcasing the optical concentration system, the behavior of monocrystalline silicon photovoltaic cells under solar concentration, and the heat transfer in the heat absorber, which

cools the cells using water. "Figure 1" illustrates the CPVT-LFR project intended to be installed on the rooftop of LEA in Brasília.

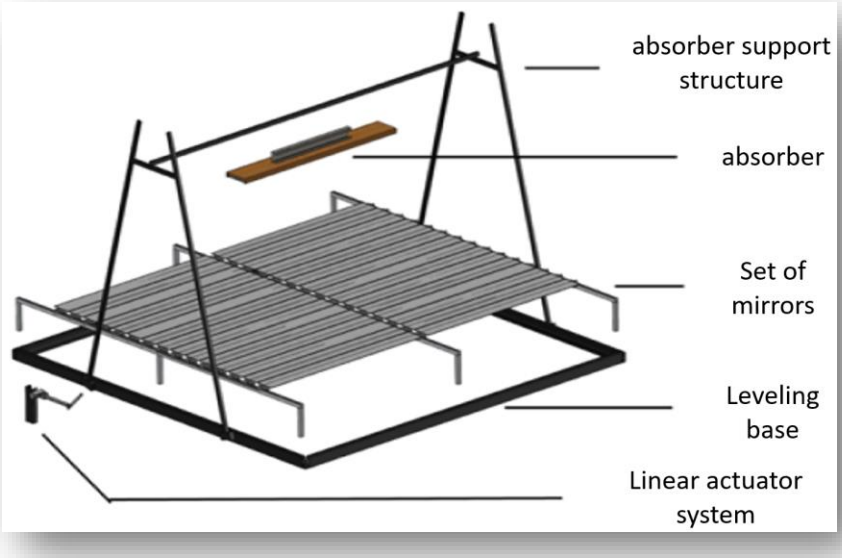

Figura 1. Design of CPVT-LFR system to LEA.

2. CPVT-LFR SYSTEM DESCRIPTION

The CPVT-LFR system to be installed in LEA consists of a solar concentrator with Linear Fresnel reflectors and a heat absorber with monocrystalline silicon photovoltaic cells. The cells are affixed to the surface of the absorber, within which water flows to cool the cells; in doing so, the water heats up, thereby acquiring thermal energy. In this way, concentration can increase the irradiance on the cells without excessively raising their temperature, which is beneficial since the efficiency of photovoltaic cells decreases at high temperatures. "Figure 2.1" shows the solar concentration on the absorber of the project in an initial test conducted at LEA-UnB.

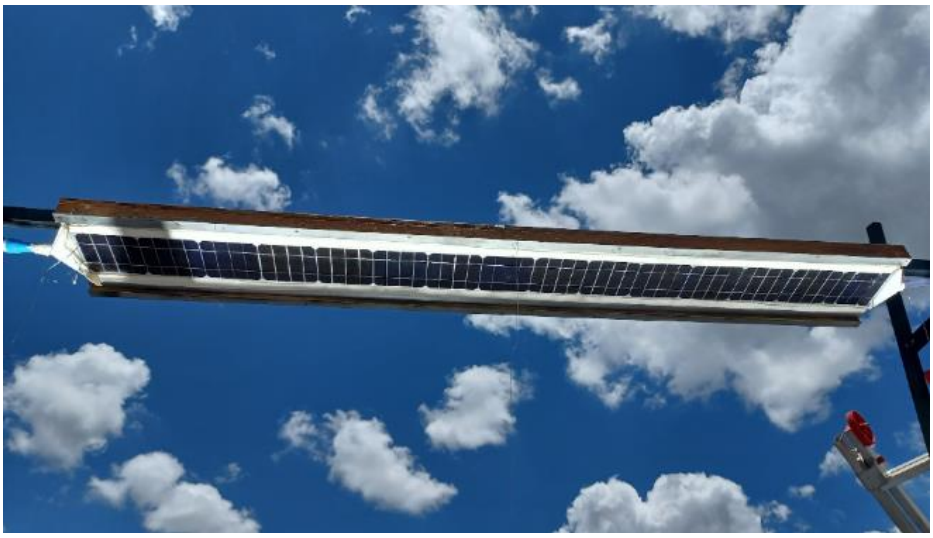

Figure 2.1. Absorber with concentrated sunlight.

2.1 Concentrator and mirrors

The solar concentrator consists of two sets of mirrors in line, with each set containing 15 flat mirrors that reflect sunlight onto the focal line where the absorber is located. Each mirror has dimensions of 2.0 x 0.2 m with a thickness of 3 mm, and there is a gap of 9 mm between the mirrors. Furthermore, it is crucial for the mirrors to move according to the Sun tracking system to concentrate solar radiation on the focal line, thus avoiding losses in optical efficiency. All

mirrors have different angles of inclination. Nevertheless, they move uniformly, following the daily movement of the Sun in relation to the Earth. Another important point is that due to the uneven structure of the rooftop, it was necessary to construct a leveling base for mirror fixation. "Figure 2.2" presents a simulation from TONATIUH (an open-source software) illustrating how solar concentration through Linear Fresnel reflectors works.

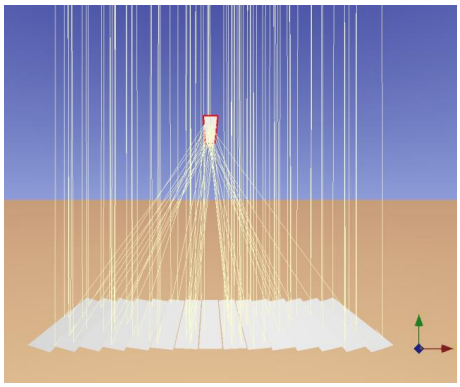

Figure 2.2. Solar Concentration with Linear Fresnel reflectors.

2.2 Heat absorber

The absorber (receiver) consists of two main parts: the monocrystalline silicon photovoltaic cells and the rectangular duct through which water will pass. The absorber has a length of 2.0 m and will be positioned at a height of 2.0 m relative to the mirrors. The cells were cut and connected in series on the absorber, maintaining a constant voltage and reducing current generation in the cut cells. A total of 12 cells were cut into 4 parts, resulting in 48 new cells connected in series on the absorber. Additionally, excepting the photovoltaic cell surface, the absorber will be thermally insulated with Styrofoam and wood. "Figure 2.3" shows various components that make up the absorber.

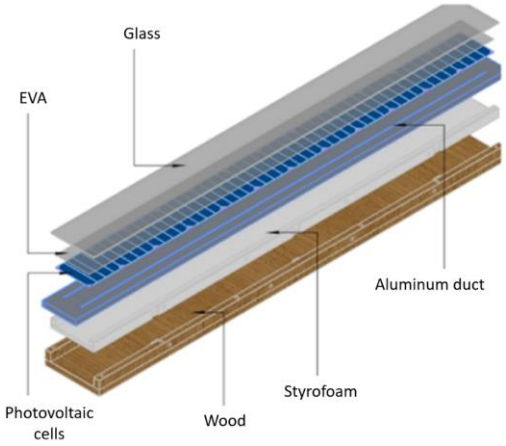

Figure 2.3. Components of the absorber.

3. OPTICAL ANALYSIS

The optical analysis aimed to determine the optical efficiency - which represents the percentage of incident solar irradiation on the mirrors that is concentrated on the absorber -, and the luminous flux uniformity. The latter is a dimensionless parameter that represents the homogeneity of solar irradiance on a specific surface and it´s defined by the ratio of the standard deviation to the mean of the incident irradiance on the surface. The irradiance is more uniform when the uniformity index value approaches 0. Furthermore, the TONATIUH software was used to perform three-dimensional geometric modeling and simulation of the solar concentration system. This software was developed by CENER (National Renewable Energy Centre, Spain) and validated by NREL (National Renewable Energy Laboratory).

Previous studies have shown that the efficiency of photovoltaic cells decreases when they are subjected to non-uniform illumination. According to Franklin and Coventry (2002), photovoltaic cells exposed to heterogeneous or non-uniform illumination from various concentrator systems experience a reduction in electrical efficiency due to a decrease

in the open-circuit voltage. This is attributed to temperature differences that arise between more and less illuminated regions.

3.1 Modeling and simulation

To perform the simulation, TONATIUH requires various input information such as location, concentrator geometry, mirror characteristics, absorber height, direct normal irradiance (DNI), among others. In this regard, it is important to note that the quality of the simulation is related to the number of solar rays used, the number of divisions of the surface where solar light is concentrated (absorber surface), and the rate of variation of solar angles - elevation angle (El) and azimuth angle (Az). Additionally, the simulation was carried out for half of the assembled structure, with the other part being symmetrical to the simulated portion. The mirrors were oriented longitudinally in the north-south direction. The input data for the modeling and simulation are presented in "Table 3.1".

Table 3.1. Input data for simulation of the concentration system in TONATIUH.

Location (LEA - UnB, Brasília - DF)	Latitude = -15,78°	Longitude = -47,93°
Number of mirrors (n)	15	-
Length x Width of mirrors ($L_{esp}\ x\ b_{esp}$)	L_{esp} = 2,0 m	b_{esp} = 0,125 m
Thickness of mirrors (e)	e = 3 mm	-
Gap between mirrors (f)	f = 9 mm	-
Reflectivity of mirrors (ρ)	ρ = 0,88	-
Height of the absorber relative to the mirrors (h)	h = 2 m	-
Length x Width of absorber ($L_{abs}\ x\ b_{abs}$)	L_{abs} = 2,0 m	b_{abs} = 0,125 m
Number of subareas of the absorber	400	-
Direct Normal Irradiance (DNI)	DNI = $1000 W/m^2$	-
Number of light rays	$3 * 10^7$	-
Variation of solar angles ($El\ e\ Az$)	5°	1368 positions

3.2 Results and analysis

TONATIUH provides the irradiance in each subarea of the absorber. So, OCTAVE was used to calculate the uniformity index and the optical efficiency. The following equations "Eq. (3.1)", "Eq. (3.2)", "Eq. (3.3)", and "Eq. (3.4)", developed by Cardoso et al. (2018) were employed for the calculation of the uniformity index,

$$I.U = \frac{\sqrt{\frac{1}{400}\left(\sum_{j=1}^{20}\sum_{i=1}^{20}\left(\Phi_{i,j}-\overline{\Phi}\right)^2\right)}}{\overline{\Phi}} \tag{3.1}$$

$$\Phi_{i,j} = \frac{N_{i,j}P_{ph}}{A_s} \tag{3.2}$$

$$A_s = |x_i - x_{i+1}| * |y_i - y_{i+1}| \tag{3.3}$$

$$\overline{\Phi} = \frac{\sum_{j=1}^{20}\sum_{i=1}^{20}\Phi_{i,j}}{400} \tag{3.4}$$

where $I.U$ is the uniformity index, $\Phi_{i,j}[W/m^2]$ is the solar irradiation in the subarea i, j, $N_{i,j}$ is the number of photons or rays that fall on that subarea, $P_{ph}\,[W]$ is the power per photon or ray, $A_s[m^2]$ is the size of the subarea, $x_i[m]$ e $y_i\,[m]$ are the coordinates of the center point of the subarea i, j, $x_{i+1}[m]$ e $y_{i+1}[m]$ are the coordinates of the center point of the neighbor subarea and $\overline{\Phi}\ [W/m^2]$ is the mean solar irradiance at the surface of the absorber.

To calculate the optical efficiency (η_{conc}) of the concentrator, the following equations were employed: “Eq. (3.5)”, “Eq. (3.6)”, “Eq. (3.7)”, “Eq. (3.8)” e “Eq. (3.9)”, the “Eq. (3.5)” was used in the study by Ajdad *et al.* (2018),

$$\eta_{conc} = \frac{\dot{Q}}{DNI * A_{conc}} \tag{3.5}$$

$$\dot{Q} = P_{ph}\sum_{i=1}^{20}\sum_{j=1}^{20}N_{i,j} \tag{3.6}$$

$$\omega_i = 90 - \frac{1}{2} tan^{-1}\left(\frac{h}{e_i} - \frac{\theta_T}{2}\right) \tag{3.7}$$

$$\theta_T = \left|tan^{-1}\left(\frac{tan(El)}{tan(Az)}\right)\right| \tag{3.8}$$

$$A_{conc} = W_{espelho} \sum_{i=1}^{15} cos\left(\omega_{i,\theta_T=90}\right) \tag{3.9}$$

where $\dot{Q}\ [W]$ is total incident power on the surface of interest, DNI $[W/m^2]$ is direct normal irradiance, $A_{conc}[m^2]$ is total aperture area of the concentrator for peak Sun, $\omega_i[°]$ is transverse rotation angle of the i-th mirror, $h\ [m]$ is height of the absorber relative to the mirrors, $\theta_T[°]$ is transverse incidence elevation angle of the Sun on the mirrors, $El\ [°]$ is solar elevation angle, $Az[°]$ is azimuth angle. The value obtained for A_{conc} was 2,78 m^2.

With this procedure, it is possible to determine the average values of optical efficiency and uniformity per hour for each month of the year at the project location. For this project, a uniformity index of 0.3 or less was defined as acceptable, which occurs during the months of December to March (between 10 AM and 3 PM) and April to November (between 10 AM and 2 PM), as shown in "Figure 3.2". This figure displays the average hourly values of optical efficiency and uniformity. Furthermore, by observing "Figure 3.2", it can be noted that between approximately 8 AM and 4 PM, the optical efficiency and uniformity index exhibit an inverse behavior - as one increases, the other decreases. "Figure 3.3" presents the distribution of irradiance on the surface of the absorber - lighter areas indicate higher levels of irradiance (above $10000 W/m^2$).

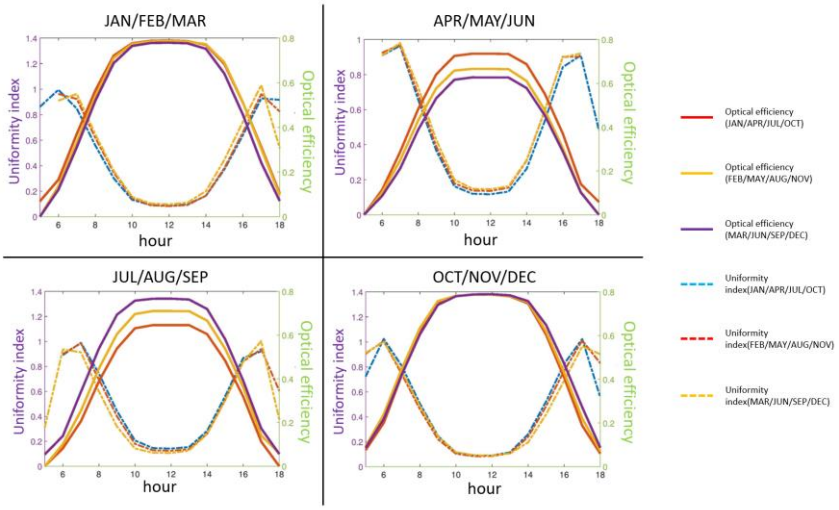

Figure 3.2. Optical efficiency and uniformity index (solid line - optical efficiency, dashed line - uniformity index).

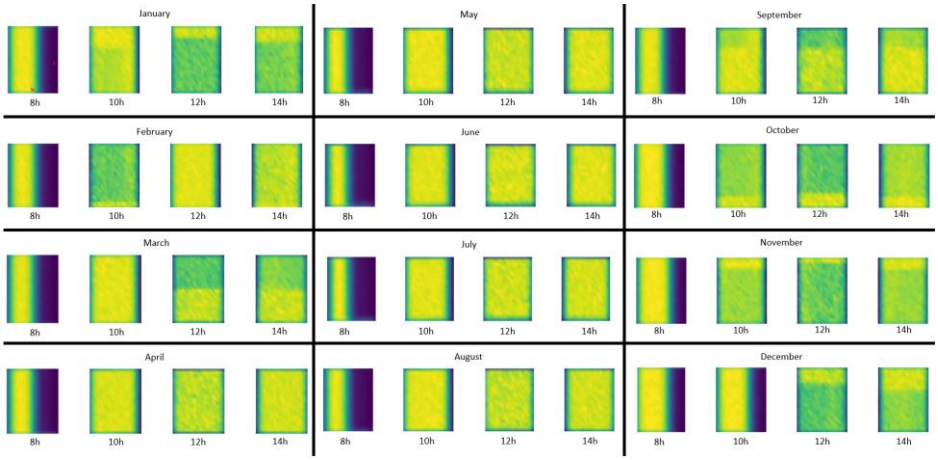

Figure 3.3. Distribution of solar irradiance on the absorber surface throughout the year (at 8 AM, 10 AM, 12 PM, 2 PM).

Analyzing "Figure 3.3," it can be observed that at 8 AM in all months of the year, the distribution of solar irradiance is heterogeneous, which can lead to losses in electricity generation. This phenomenon is due to the shadowing of mirrors by their neighbors at this time of day, resulting in the concentration of irradiance on only one side of the absorber.

To account the variation in uniformity in the general model of CPVT-LFR, the incidence angle modifiers method was employed. This method involves determining values (between 0 and 1) that, when multiplied by the efficiency at the zenith, provide the optical efficiency in the analyzed subarea ("Eq. (3.10)"). Thus, the incidence angle modifiers vary with the position of the Sun, with a value of one when the Sun is at the zenith. These values were determined based on the optical efficiency data obtained from the simulation in TONATIUH and processed in OCTAVE. "Figure 3.4" illustrates these modifiers in some subareas of the absorber. Moreover, this procedure enables the determination of irradiance in each subarea of the absorber using only the information of direct normal irradiance (DNI), solar azimuth, and elevation.

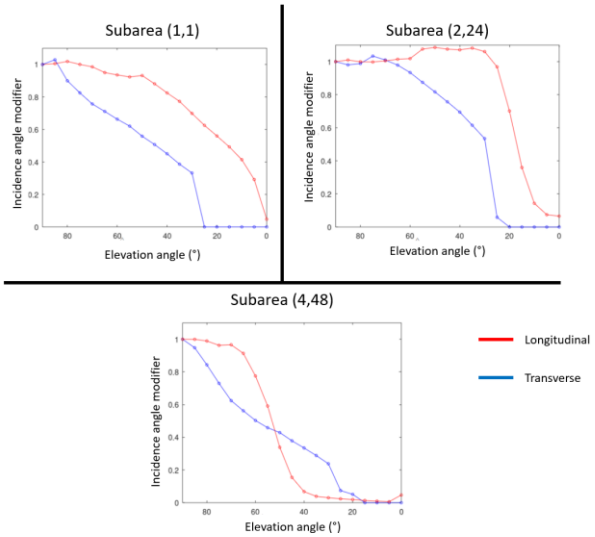

Figure 3.4. Incidence angle modifier in some subareas of the absorber (blue - longitudinal, red - transverse).

$$\eta_{conc,i,j} = \left(\eta_{conc,i,j,z\hat{e}nite}\right) * IAM_L * IAM_T \tag{3.10}$$

where $\eta_{conc,i,j}$ is optical efficiency in subarea i,j; $\eta_{conc,i,j,z\hat{e}nite}$ is optical efficiency in subarea i,j at the zenith ($El = 90°$ e $Az = 0°$); IAM_L is longitudinal incidence angle modifier e IAM_T is transverse incidence angle modifier.

Finally, the maximum value of optical efficiency obtained for the system was 0.79. Comparing this value with the maximum optical efficiency of 0.525 achieved in the study by Gadioli de Souza (2019), which utilized a tubular absorber, it can be inferred that using a flat absorber instead of a tubular one increases the optical efficiency of the system.

4. THERMAL ANALYSIS

The thermal analysis involved the determination of temperature variation in the cooling fluid of photovoltaic cells and calculating the thermal efficiency, which represents the amount of thermal energy absorbed by the fluid relative to the concentrated radiation on the absorber. In this perspective, the analysis of heat transfer in the absorber is highly relevant, since faster heat transfer results in more uniform cell temperatures and reduced loss of electrical efficiency.

4.1 Modeling and simulation

Heat transfer analysis was done using the method of thermal resistances, and since thermal transient is important, capacitances are used to represent it. The model is based on the works of Karathanassis et al. (2019) and Monteiro Filho (2018). To calculate the energy input into the system, the model utilizes the previously determined optical efficiency and direct normal irradiance (DNI) data. The absorber is then discretized into control volumes (CV) in the longitudinal direction, and the energy balance equation is applied to each component (glass, photovoltaic cells, lower face of the duct, cooling fluid) in each CV using implicit finite differences. "Figure 4.1" presents the longitudinal and transverse views of the absorber, with the longitudinal view showing the temperatures involved in the problem, which are detailed in "Table 4.1". Meanwhile, "Figure 4.2" shows the thermal circuit for the absorber.

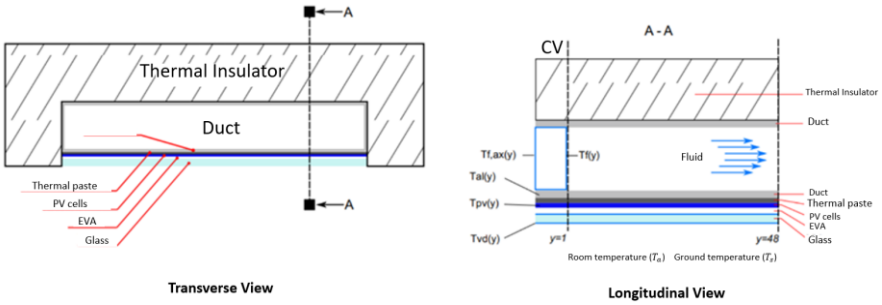

Figure 4.1. Transverse and longitudinal cross-sectional views of the absorber.

Table 4.1. Temperatures involved in the heat transfer in the absorber.

Variable	Meaning
T_a	Room temperature
T_s	Ground temperature
T_{vd}	Glass temperature
T_{pv}	Photovoltaic cell temperature
T_{al}	Temperature of the lower face of the aluminum duct
$T_{f,ax}$	Temperature of the fluid in the previous control volume
T_f	Fluid temperature

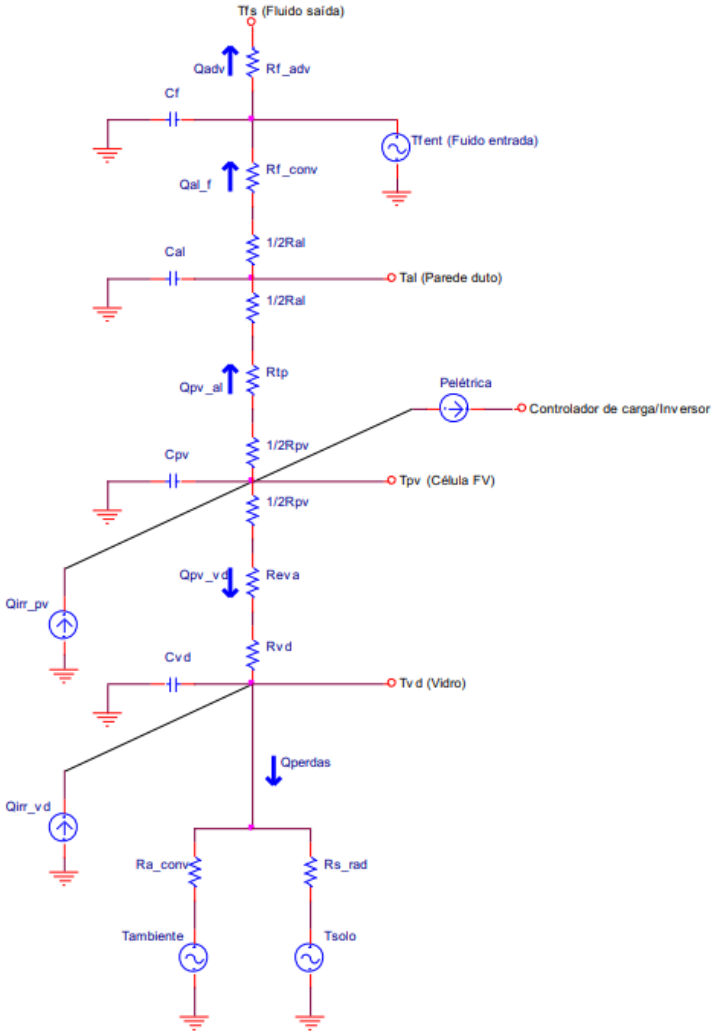

Figure 4.2. Thermal circuit of the absorber.

By applying "Eq. (4.1)" - the energy balance equation - to the elements of the absorber in control volumes (CV) along the longitudinal direction, a system of nonlinear equations is obtained, which is solved using the Newton-Raphson method implemented in OCTAVE,

$$\frac{d(E_{sistema})}{dt} = (\dot{Q}_e - \dot{Q}_s) + (\dot{W}_e - \dot{W}_s) + \dot{m}_e * h_e - \dot{m}_s * h_s \quad (4.1)$$

where $\frac{d(E_{sistema})}{dt}$ $[W]$ is temporal variation of the system's energy, $\dot{Q}_e[W]$ is inlet heat flow in the system, $\dot{Q}_s[W]$ is outlet heat flow in the system, $\dot{W}_e[W]$ is inlet power in the system, $\dot{W}_s[W]$ is outlet power in the system, h_e[kJ/kg] is enthalpy of the inlet fluid, h_s[kJ/kg] is enthalpy of the outlet fluid, $\dot{m}_e$[kg/s] is mass flow of the inlet fluid and $\dot{m}_s$[kg/s] is mass flow of the outlet fluid.

For example, by applying the equation above to the cooling fluid of the photovoltaic cells, the thermal balance in the fluid is represented by "Eq. (4.2)",

$$M_f * c_f * \frac{T_f - T_{f,a}}{\Delta t} = \frac{T_{pv} - T_d}{R_{f,d}} - \dot{m}_f * c_f * (T_f - T_{f,ax}) \quad (4.2)$$

where $M_f[kg]$ is fluid mass relative to control volume, $c_f[J/kg * K]$ is specific heat of the fluid, $T_f[°C]$ is fluid temperature, $T_{f,a}[°C]$ is fluid temperature at the previous time step, $T_{f,ax}[°C]$ is temperature of the fluid in the previous control volume, $T_{pv}[°C]$ is photovoltaic cell temperature, $T_d[°C]$ is duct temperature, $R_{f,d}[°C/W]$ is thermal resistance between the fluid and the duct, and $\dot{m}_f[kg/s]$ is fluid mass flow. The equations for the other elements of the absorber are detailed in the work of Fantini (2021).

To solve the equations, it is necessary to know various geometric and physical characteristics of the CPVT-LFR, such as layer thicknesses, thermal conductivity, absorptivity, specific heat capacity, etc. Additionally, the calculations were performed for a mass flow rate ranging from 0.01 to 0.1 kg/s, and the absorber was divided into 48 longitudinal elements. These data are provided in "Table 4.2."

Table 4.2. Geometric and physical characteristics of the CPVT-LFR

.

Concentrator aperture área	$2{,}767m^2$	Glass thermal conductivity	$1{,}4W/mK$
Absorber width	$0{,}125m$	PV cell thermal conductivity	$148W/mK$
Absorber length	$2{,}0m$		
Absorber height	$2{,}0m$	EVA thermal conductivity	$0{,}35W/mK$
		Thermal paste thermal conductivity	$1{,}2W/mK$
Number of photovoltaic cells	48	Aluminum density	$2697kg/m^3$
Thickness of photovoltaic cells	$170\mu m$	PV cell density	$2330kg/m^3$
Glass thickness	$3{,}0mm$	Glass density	$2230kg/m^3$
EVA thickness	$0{,}5mm$	Aluminum specific heat	$900J/kgK$
Aluminum thickness	$1{,}0mm$	PV cell specific heat	$712J/kgK$
Thermal paste thickness	$0{,}6mm$	Glass specific heat	$830J/kgK$
PV cell absorptivity	0,92		
Glass emissivity	0,9		
Glass+EVA emissivity	0,82		
Glass+EVA absorptivity	0,18		

4.2 Results and analysis

Solving the thermal balance equations, temperature values of interest are obtained, such as the fluid temperature at the outlet and the temperature of the photovoltaic cells. "Figure 4.4" illustrates the variation in outlet fluid temperature as a function of mass flow rate and the variation in cells temperature along the longitudinal direction of the absorber, where 0 refers to the cell at the absorber's inlet, and 50 refers to the cell at the outlet. Analyzing "Figure 4.4," it can be observed that the temperature of the photovoltaic cells remained below 100°C for any flow rate values, and higher flow rates resulted in a more uniform temperature distribution across the absorber cells. Additionally, it is noticeable that the outlet fluid temperature decreases with an increase in the mass flow rate.

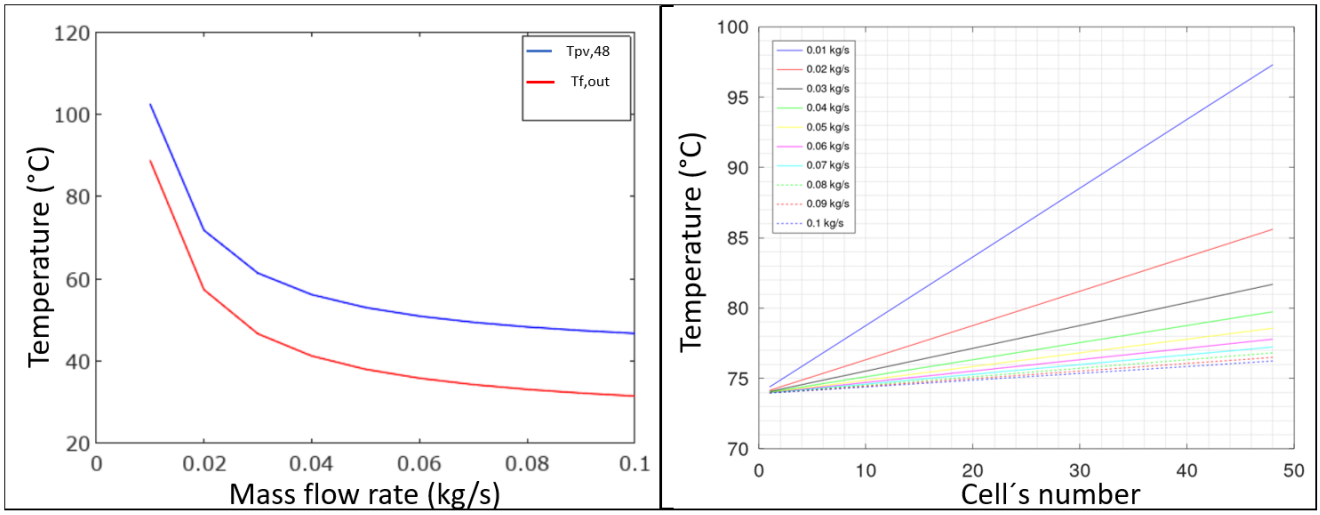

Figure 4.4. Outlet fluid temperature (left) and photovoltaic cell temperature (right).

With the temperature data, it is possible to obtain the thermal and electrical efficiencies using the equations "Eq.(4.3)" e "Eq.(4.4)",

$$\eta_t = \frac{\dot{m}_f * c_f * (T_s - T_e)}{\eta_{conc} * DNI * A_{conc}} \tag{4.3}$$

$$\eta_{ele} = \frac{P_{el}}{DNI * A_{conc}} \tag{4.3}$$

where η_t is thermal efficiency, η_{ele} is electrical efficiency, $P_{el}[W]$ is electrical power generated by cells, $\dot{m}_f[kg/s]$ is fluid mass flow rate, c_f $[J/kg * K]$ is specific heat of fluid, $T_s[°C]$ outlet fluid temperature, $T_e[°C]$ is inlet fluid temperature, η_{conc} is optical efficiency of concentrator, $DNI[W/m^2]$ is direct normal irradiance, $A_{conc}[m^2]$ is total aperture area of the concentrator.

The graphs of electrical and thermal efficiency as a function of mass flow rate are presented in "Figure 4.5". Analyzing these graphs, it is known that higher mass flow rates result in more uniform cell temperatures, thereby reducing electrical efficiency losses. However, higher mass flow rates also lead to lower fluid temperature at the system outlet, consequently resulting in lower thermal efficiency. Thus, electrical, and thermal efficiencies exhibit inverse behaviors with respect to the mass flow rate of the cooling fluid. Furthermore, it is inferred that the obtained electrical efficiency values range from 8.5% to 10%, while the thermal efficiency values range from 79% to 83%, indicating that a significant portion of the incident irradiation on the absorber is converted into heat.

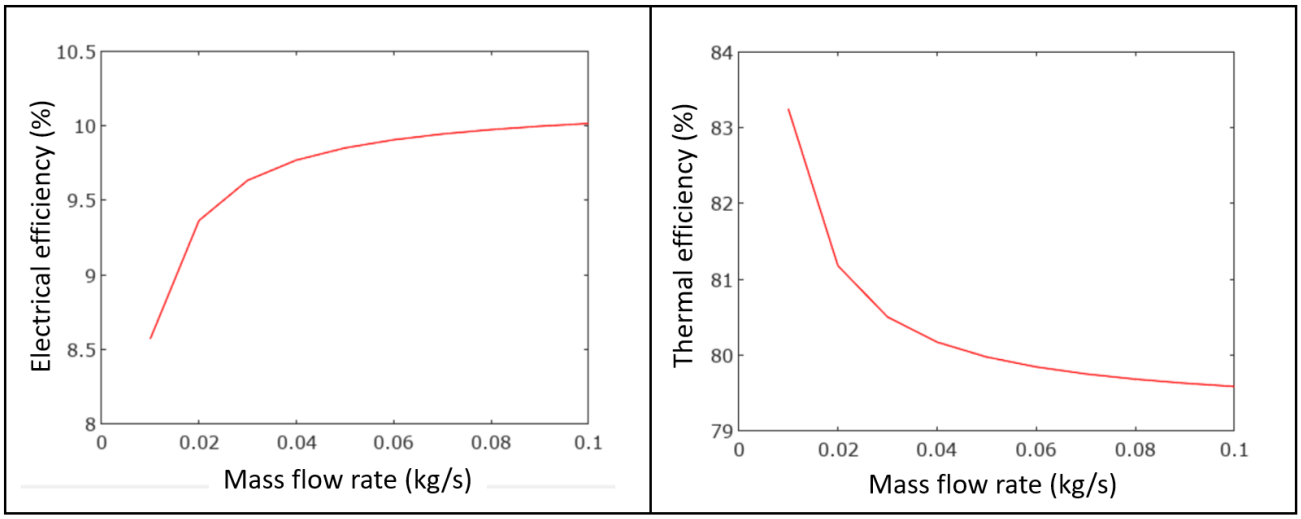

Figure 4.5. Electrical efficiency (left) and thermal efficiency (right) of the system as a function of water mass flow rate.

5. CONCLUSION

Based on the above, it is evident that the hybrid photovoltaic-thermal system using Linear Fresnel reflectors offers the advantage of generating two forms of energy (electricity and heat) compared to traditional photovoltaic systems. However, the construction and cost of the CPVT-LFR system are drawbacks compared to traditional photovoltaic systems. Another interesting point is that the electrical efficiency obtained in this system is lower than that of photovoltaic panels. The maximum electrical efficiency obtained was 10%, while the thermal efficiency reached 83%. The cell temperature remained below 100°C, and the outlet fluid temperature could exceed 40°C.

Furthermore, a CPVT-LFR prototype was built at the LEA and tests were conducted to evaluate the system's concentration. In this phase, the precision of the linear actuator for solar concentration was assessed to ensure uniform luminosity on the absorber, and the results were positive as shown in "Figure 2.1".

6. ACKNOWLEDGEMENTS

We thank Faculdade de Tecnologia da Universidade de Brasília and to the various members of the Energy and Environment Laboratory (LEA) for their direct or indirect contributions that made this work possible. We would also like to thank FAP-DF for financially supporting the project number 00193.0000226/2019-72 through their program for promoting scientific, technological, and innovative research projects.

7. REFERENCES

Ajdad, H., et al. "Thermal and optical efficiency analysis of the linear fresnel concentrator compound parabolic collector receiver." *Journal of Solar Energy Engineering* 140.5 (2018): 051007.

Cardoso, João P., et al. "New functionalities for the Tonatiuh ray-tracing software." *AIP Conference Proceedings*. Vol. 2033. No. 1. AIP Publishing, 2018.

Energy, Global. "Global Energy & CO2 Status Report." *International Energy Agency: Paris, France* (2019).

Fantini, Darío Gerardo. "Estudo teórico de um sistema híbrido fotovoltaico térmico com concentrador refletor linear Fresnel." (2021).

Franklin, E., and J. Coventry. "Effects of highly non-uniform illumination distribution on electrical performance of solar cells." (2002).

Karathanassis, I. K., et al. "Dynamic simulation and exergetic optimization of a Concentrating Photovoltaic/Thermal (CPVT) system." *Renewable Energy* 135 (2019): 1035-1047.

Lewis, Nathan S. "Toward cost-effective solar energy use." *science* 315.5813 (2007): 798-801.

Monteiro Filho, Arthur. "Hibridização de gás confinado em depósitos de resíduo sólido urbano com heliotérmica para geração de energia: o caso do Lixão da Estrutural no DF." (2018).

Pereira, Enio Bueno, et al. "Atlas brasileiro de energia solar." *São josé dos campos: Inpe* 1 (2017).

Sousa, João Pedro Gadioli de. "Análise da transferência de calor em concentrador solar do tipo Fresnel linear de tubo evacuado: estudo da pressão." (2019).

8. RESPONSIBILITY NOTICE

The authors are the only responsible for the printed material included in this paper.